Hydrogen and Oxygen Adsorption on Rh$_n$ (n = 1−6) Clusters

Daniela S. Mainardi and Perla B. Balbuena*

Department of Chemical Engineering, University of South Carolina, Columbia, South Carolina 29208

Received: July 17, 2003; In Final Form: September 30, 2003

Density functional theory is used to study electronic and physical properties of pure Rh$_n$ (n = 1−6) clusters in their ground state and those of their closest states. Optimized equilibrium bond lengths and angles, absolute and binding energies, charge distributions, and Mulliken populations are determined. The clusters chemistry is tested via adsorption of atomic oxygen and hydrogen, where a systematic study of the preferred adsorbate adsorption site is performed. Bridge sites are the preferred ones in most cases for oxygen adsorption in small rhodium clusters. The case of hydrogen is less conclusive; the small size of the adsorbate may favor top or bridge sites depending on the metal cluster morphology. Details of the interactions of metal cluster−adsorbate are analyzed via the distribution of electronic population and charge transfer.

1. Introduction

In many cases, the active components of dispersed metal catalysis are small clusters, and therefore, the cluster properties, rather than the bulk properties, are responsible for their particular characteristics. Thus, theoretical and experimental studies of clusters are very useful for the understanding and prediction of the local chemistry. Clusters have distinct properties due to a quite large surface-to-volume ratio, and as the size is reduced, their properties change drastically. For instance, clusters of nonmagnetic solids are found to be magnetic.[1−3] Hence, a systematic study of small metal clusters is needed for understanding electronic, chemical, and physical properties, such as sintering, adsorption to substrates, and catalysis effects. In particular, theoretical methods based on solutions to the Schrödinger equation[4−6] provide accurate characterization of cluster structures.

Rhodium, well-known by its catalytic properties,[7] is a common constituent of the catalyst used for the simultaneous conversion of carbon monoxide, nitrogen oxides, and hydrocarbons in automobile exhausts. The catalytic activity of Rh is in some cases enhanced when the metal is present in thin films or as small clusters. For example, a monolayer of Rh on top of a Pt layer deposited on Rh(100) has shown a higher activity toward the reduction of NO than that of the Rh(100) bare surface.[8] Small clusters, which are also used as catalysts, have been the focus of extensive investigations,[2,9−13] such as CO dissociation on rhodium supported on alumina where a strong dependence on the particle size of the Rh clusters has been reported.[14] Insights into the electronic structure and magnetism of small (less than 20 atoms) rhodium clusters,[2,10,12] as well as on the effect of the cluster size on ionization potentials, electron affinities, binding energies, and magnetic moments,[13] have been provided.

The adsorption of atoms and small molecules on rhodium surfaces has been studied to elucidate the effect of surface oxides or other impurities that significantly alter the physical and chemical properties of metal surfaces. Ab initio calculations of hydrogen adsorption on (100) surfaces of palladium and rhodium[15] reported atomic hydrogen adsorption on hollow or bridge sites with similar adsorption energies of 2.78 and 2.62 eV, respectively, and equilibrium bonding distances from the adsorbate to each of these sites of 0.38 and 1.15 Å, respectively. With the use of self-consistent scattering theory, a single H adatom was predicted to bind in a 4-fold hollow at a height of 2.46 Å above a Rh(001) layer.[16] Studies on the adsorption of H$_2$ on a Rh(001) surface suggested the interaction of each H atom with a 2-fold bridge site.[16] A systematic study of the chemisorption of atomic H and O on Rh(111) using self-consistent, periodic density functional theory (DFT) calculations[17] yielded preference for 3-fold sites for both adsorbates. Experimental studies on Rh(100) also suggest that the preferred H adsorption site is hollow.[18]

Similar studies on the adsorption of oxygen on rhodium surfaces[19−22] suggest that atomic oxygen binds both on bridge and hollow sites of rhodium surfaces. Theoretical analysis of a seven-layer Rh(111) slab[23] showed, at all coverages, that the fcc-hollow site is more stable than the hcp-hollow site for the adsorption of oxygen, and different oxygen adsorption stable patterns were found depending on the surface coverage. Results from low-energy electron diffraction (LEED) I−V experiments on Rh(100) with the (2 × 2)-2O system[19] showed that the preferred adsorption site for oxygen is a rather unusual hollow site regarded as a "pseudo-bridge", in agreement with results from ab initio calculations[20] where bridge sites were found to be the preferred sites. Other theoretical reports[22] indicate that oxygen prefers hollow sites in a (2 × 2) arrangement at low coverages (below 0.3 ML), whereas at high coverages, O atoms occupy bridge sites because of the presence of repulsive lateral interactions. The same authors also report that the bridge site is indeed ∼0.3 eV less stable than the hollow site. In summary, it appears that the preferred adsorption sites for H or O on Rh surfaces are not unique, and regarding clusters, small variations in their geometry can lead to more than one adsorption configuration of very similar energies.

We present density functional theory (DFT) fully optimized geometries of Rh$_n$, Rh$_n$−O, and Rh$_n$−H clusters (n = 1−6), including information about the most stable geometries, absolute and binding energies, Mulliken charges, and adsorption characteristics of H and O as a function of cluster size and adsorption site.

* To whom correspondence should be addressed. E-mail: balbuena@engr.sc.edu.

Methodology

We have used DFT techniques[24,25] combined with effective core potentials. The Los Alamos National Laboratory's (LANL) basis set with effective core potentials (ECP) of double-ζ type[26,27] was used along with the functional B3PW91.[28−31] The chosen functional (B3PW91), one of most successful hybrid functionals,[24] includes a exchange description constituted by contributions of local, nonlocal (Becke 3), and Hartree−Fock exchange terms, and correlation given by the PW91 nonlocal GGA functional. The use of pseudopotentials with relativistic corrections has been widely demonstrated to be a good compromise to the alternative use of full-electron procedures, which reduces the required computational effort without loss of accuracy.[32] Additional tests in the smallest clusters were performed with B3LYP/LANL2DZ and Møller−Plesset perturbation theory (MP2).[33] Calculations were performed using the Gaussian 98 program,[34] with the Berny algorithm in redundant internal coordinates[35] for geometry optimizations. Frequency calculations were performed to determine the zero-point energy and to confirm that the states were local minima.

3. Results and Discussion

3.1. Rhodium Clusters. The calculated (B3PW91/LANL2DZ) ground state for Rh is a quartet, ^4F ($4d^8 5s^1$) with five α and three β electrons in the 4d orbital, in agreement with spectroscopic results.[36] The calculated first excited state, ^2D ($4d^9$) is 0.27 eV above the ground state, whereas the experimental difference is 0.41 eV.[36] Both MP2/LANL2DZ and B3LYP/LANL2DZ yield also the quartet as ground state for the Rh atom with values of 0.63 and 0.40 eV, respectively, for the energetic difference between the first excited and the ground states. Previous calculations using LSDA and GGA along with effective core potentials[2,10] had failed to give the correct ground state; the discrepancy was attributed to limitations of the exchange-correlation description. For this reason, as discussed below, their reported binding energies are overestimated because the reference is a higher energy state of the Rh atom.

The spin multiplicity, equilibrium bond lengths and angles, zero-point energies (ZPE), absolute energies (including ZPE), cluster optimized structures, and binding energies per atom (BE/atom) corresponding to Rh$_n$ ($n = 1-6$) ground states are reported in Table 1. Binding energies per atom, calculated as BE/atom(Rh$_n$) = ($E_{Rh_n} - nE_{Rh}$)/n, increase as the number of atoms in the cluster increases, being far from the value of the cohesive energy of Rh metal, -5.75 eV, obtained for Rh$_{37}$ according to recent studies.[37]

The predicted ground-state spin multiplicity for Rh$_2$ was found to be a quintet, in agreement with previous theoretical predictions using DFT and CI methods.[2,13] There is no agreement among the variety of theoretical[2,13] and experimental values reported for the dissociation energy of Rh$_2$.[38] Our calculated (B3PW91/LANL2DZ) dimer dissociation energy ($-E_{Rh_2} + 2E_{Rh}$, which is equivalent to the spectroscopic dissociation energy[39]) is 1.50 eV, in reasonable agreement with experimental results of 1.46 ± 0.22 eV,[40] and 1.4 ± 0.3 eV[39] obtained by mass and Raman spectroscopy, respectively. However, it is well below other experimental values, such as 2.92 eV obtained from Knudsen effusion measurements,[41] and another spectroscopic value of 2.40 eV.[38] In relation to this apparent controversy, Wang et al.[39] suggest that it is possible that the ground state of Rh$_2$ may dissociate into excited states of the atoms. As summarized by Reddy et al.,[2] some theoretical values are also much higher compared with our result, but these values may be artificially overestimated because of their failure of finding

the correct ground state. On the other hand, the calculated equilibrium bond length is 2.30 Å, in good agreement with the experimental value of 2.28 Å,[40] and the associated Rh−Rh stretching frequency for the ground-state dimer is 289 cm^{-1} (scaling factor of 0.9573[42] has been applied), on the order of experimental values of 267[40] and 284 ± 19[39] cm^{-1}. Other local minima obtained with the same method/basis set were found well above the ground state; for example, for a state of spin multiplicity 3, the energy difference with the ground state is 1.07 eV. We also performed calculations using MP2/LANL2DZ, which yielded a dimer ground state of multiplicity 7 (BE/atom = -0.67 eV and bond length 2.36 Å), the quintet being the first excited state of 0.1 eV above the ground state, whereas B3LYP/LANL2DZ resulted in a quintet ground-state dimer (BE/atom = -0.75 eV and bond length 2.32 Å). Thus, although the controversy about the dimer dissociation energy remains, the results on the Rh atom and dimer and comparisons with higher level methods as MP2 give us confidence on the functional/basis set adopted in this study.

The ground-state Rh$_3$ cluster (Table 1) is a sextet isosceles triangle with C_{2v} symmetry and a binding energy per atom of 1.33 eV. Previous calculations reported either the C_{2v} (sextet or quartet)[2,43] or a D_{3h} (quartet)[13] ground state with binding energies per atom varying within a wide range, some of them overestimated because of the use of a higher energy state for the ground state of the Rh atom. For example, for the same spin multiplicity and symmetry, a value of -1.94 eV was reported using GGA.[44] Our calculations yielded a state of multiplicity 4, 0.13 eV less stable than the ground state; it is also an isosceles triangle of Rh1−Rh2 = Rh1−Rh3 = 2.51 Å and Rh2−Rh3 = 2.74 Å.

The ground-state found for Rh$_4$ is a spin singlet tetrahedron (Table 1) with a bond length of 2.48 Å and a binding energy of 1.66 eV/atom. Similar geometries (singlets for tetrahedrons and quintets for squares) were reported earlier[2,44] with bond lengths ranging between 2.38 and 2.50 Å and BE/atom from 2.35 to 2.91 eV/atom using GGA.[2]
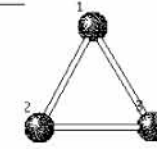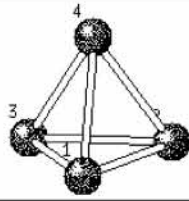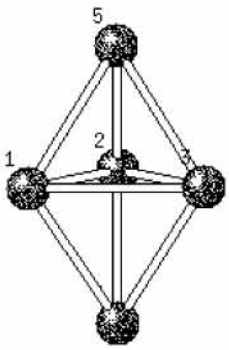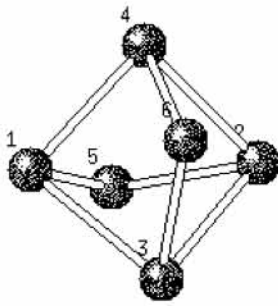
For Rh$_5$, the calculated ground state is a spin quartet with distorted triangular-bipyramid geometry (Table 1) and a binding energy of 1.80 eV/atom, in contrast with previous reports for a square pyramid (octet) with a binding energy of 3.11 eV/atom[2] and a sextet state of the same geometry 0.02 eV above the ground state, whereas a triangular bipyramid structure with multiplicity 4 was found to be 0.35 eV less stable than the square pyramid geometry.

A C_1 ground-state structure corresponding to Rh$_6$ (Table 1) is a slightly distorted square bipyramid. It is a singlet with a binding energy of -1.86 eV/atom, whereas GGA studies[2] yielded D_{4h} symmetry singlet with higher binding energy of -3.28 eV/atom, where the reference was the ^2D state for the Rh atom. We found other geometries (triplet and quintet) for Rh$_6$ lying 0.28 and 0.34 eV above the singlet state.

As shown here, the complexity of their electronic states induces a variety of low-lying electronic states in transition metal clusters. In comparison with previous studies with the same method/basis set, we found that Rh clusters with an even number of atoms (closed shell configurations) are found in the same ground-state geometry as the corresponding platinum clusters.[45] The geometries of Rh clusters with an odd number of atoms (open shell configurations) presented here were also found for Pt clusters;[45] however, these were not the ground states for those Pt clusters.

3.2. Rhodium−Adsorbate (H, O) Clusters. Tables 2 and 3 show the spin multiplicity, optimized (B3PW91/LANL2DZ)

TABLE 1: Spin Multiplicity, Equilibrium Bond Lengths and Angles, Zero-Point Energies (ZPE), Absolute Energies (including ZPE), Cluster Optimized (B3PW91/LANL2DZ) Structures, and Binding Energies (BE) Per Atom, for Pure Rh$_n$ ($n = 1-6$) Clusters

System	m	Bond Length (Å) Angle (°)	ZPE (Ha)	E +ZPE (Ha)	Geometry	−BE (eV/ atom)
Rh	4			-109.47505		
Rh$_2$	5	1-2 = 2.30	0.000687	-219.00528		0.75
Rh$_3$	6	1-2 = 1-3 = 2.51 2-3 = 2.38 1-2-3 = 61.7 2-1-3 = 56.6	0.001348	-328.57224		1.33
Rh$_4$	1	1-2 = 1-3 = 2.48 1-3 = 1-4 = 2.48 1-4 = 2-4 = 2.48 2-3 = 2.48 3-4 = 2.48 angles = 60.0	0.003055	-438.14464		1.66
Rh$_5$	4	1-2 = 2.60 1-3 = 2-3 = 2.60 1-4 = 2.59 1-5 = 3-5 = 2.52 2-4 = 3-4 = 2.59 2-5 = 2.52 5-4 = 4.14 1-2-3 = 2-3-1 = 60.0 1-5-2 = 2-5-3 = 62.2 5-1-2 = 5-3-2 = 58.9 1-5-3 = 62.1 1-4-3 = 60.4	0.003020	-547.70685		1.80
Rh$_6$	1	1-2 = 3-4 = 3.43 1-3 = 1-4 = 2.46 1-5 = 2.47 1-6 = 3-5 = 2.80 2-3 = 2-4 = 2.46 2-5 = 3-6 = 2.47 2-6 = 5-4 = 2.80 5-6 = 4.00 1-2-3 = 45.9 2-3-1 = 88.3 1-5-2 = 87.7 5-1-2 = 46.2 2-5-3 = 1-5-3 = 55.2 5-3-2 = 55.7 6-5-3 = 37.8 1-4-3 = 45.7	0.004816	-657.25955		1.86

bond lengths and angles, ZPE and absolute energies, and binding energies for optimized Rh−H and Rh−O clusters. Binding energies are calculated using eq 1:
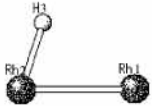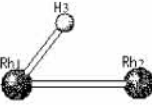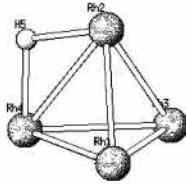
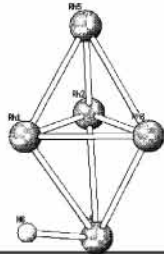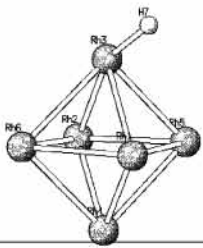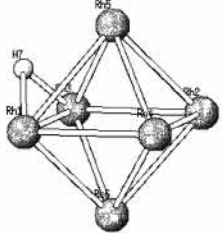$$BE(Rh_nX) = (E_{Rh_nX} - E_{Rh_n} - E_X) \qquad (1)$$

where X denotes the adatom, H or O. Whenever the metal cluster geometry allowed it, top, bridge, and hollow sites were tested upon adsorption of H and O on Rh$_n$ ($n = 1-6$) clusters.

The ground state corresponding to Rh−H cluster is a triplet with a bond length of 1.63 Å (Table 2) and a Rh−H stretching frequency of 1713 cm^{-1} (scaling factor of 0.9573[42] has been applied). A singlet state is also a local minimum with an energy

difference of 0.03 eV with respect to the ground state. There are very few reported calculated and experimental data regarding geometries or binding energies for these systems. Nayak et al.[44] reported calculated values of adsorption of H$_2$ to Rh$_2$ and Rh$_4$, where H$_2$ dissociates and adsorbs as atomic H. Their reported Rh−H bond length of 1.53 Å for H$_2$ attached to a single Rh atom is 0.10 Å shorter than that found for RhH.

Two optimized geometries were found for Rh$_2$−H (Table 2), both of the same multiplicity, doublets. In one of them, H is located on top of one Rh atom in the Rh$_2$ cluster, and in the other, H occupies a bridgelike site, which we designate as "tilted top". Rh$_2$−H tilted top is the most stable of these geometries with a binding energy per atom 0.02 eV higher than that of

TABLE 2: Spin Multiplicity, Cluster Optimized Geometries, Equilibrium Bond Lengths and Angles, ZPE, Absolute Energies (including ZPE), Atomization, and Binding Energies (BE) for Optimized (B3PW91/LANL2DZ) Rh$_n$–H ($n = 1-6$) Clusters[a]

System	m	Geometry	Bond Length (Å) Angle (°)	ZPE (Ha)	E+ZPE (Ha)	−BE (eV)
Rh-H	3		**1.63**	0.004076	-110.06368	**2.27**
Rh$_2$-H Top	2		1-2 = 2.53 **2-3 = 1.55** 1-3 = 2.55 3-2-1 = 72.7	0.00602	-219.61188	2.88
Tilted top	2		1-2 = 2.55 **1-3 = 1.61** 2-3 = 2.02 3-1-2 = 52.3	0.005378	-219.61233	**2.89**
Rh$_4$-H Bridge	4		1-2 = 2-3 = 2.53 2-4 = 2.71 1-3 = 2.42 1-4 = 2.64 **2-5 = 1.67** **4-5 = 1.74** 1-5 = 3.11 5-2-4 = 38.5	0.00865	-438.74279	2.64
Rh$_5$-H Tilted Top	1		1-2 = 2.46 1-3 = 2.46 2-3 = 2.46 2-4 = 2.61 3-5 = 2.55 **4-6 = 1.60** 1-6 = 1.97 6-4-1 = 44.6	0.010159	-548.28367	**2.06**
Rh$_6$-H Top	2		1-3 = 2.53 1-5 = 2.60 2-3 = 2.70 2-5 = 2.53 4-6 = 2.58 **7-3 = 1.59** 7-1 = 2.79 7-5 = 3.27	0.01072	-657.88037	3.26
Bridge	4		1-3 = 2.76 1-4 = 2.60 2-3 = 2.59 2-5 = 2.61 4-6 = 2.59 **7-1 = 1.80** 7-5 = 2.04 **7-3 = 1.74**	0.010127	-657.88714	**3.44**
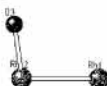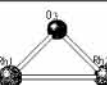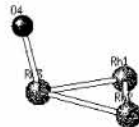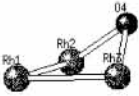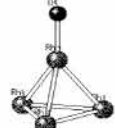
[a] Shortest Rh−H bond distances and BE for the most stable states are indicated in bold.

on-top adsorption. The Rh−Rh distance increases from 2.30 (Rh$_2$, Table 1) to 2.53 Å for the adsorption on top and to 2.55 Å for the tilted top case, indicating that binding to H is made at expenses of the Rh−Rh bond weakening.
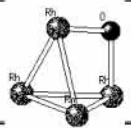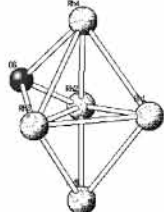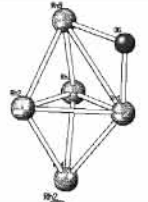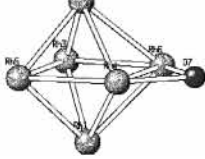
No stable structures were found for H adsorption on-top, bridge, or hollow sites of Rh$_3$, although many different initial configurations were tried. We do not have an explanation for this, and unfortunately, there are no other published experimental or theoretical reports of Rh$_n$H and Rh$_n$O that we are aware of, except for Rh$_6$H that we discuss below. For Rh$_4$−H and Rh$_5$−H, the ground states reveal both bridge and tilted top H bonding to the Rh atoms, respectively. The spin multiplicity found for Rh$_4$−H was a quartet and for Rh$_5$−H a singlet. Almost all bond lengths of the tetrahedron Rh$_4$ are 2.48 Å (Table 1); however, when H adsorbs on one of its bridge sites (Rh2−Rh4, Table 2), all Rh−Rh bond lengths are elongated, especially that corresponding to the bridge site (2.71 Å). This Rh−Rh bond elongation is qualitatively in agreement with that found by

TABLE 3: Spin Multiplicity, Cluster Optimized Geometries, Equilibrium Bond Lengths and Angles, ZPE, Absolute Energies (including ZPE), Atomization, and Binding Energies (BE) for Optimized (B3PW91/LANL2DZ) Rh$_n$−O (n = 1−6) Clusters[a]

System	m	Geometry	Bond Length (Å) / Angle (°)	ZPE (Ha)	Energy (Ha)	−B.E (eV)
Rh-O	4		**1.76**	0.001872	-184.65527	**3.49**
Rh$_2$-O Top	3		1-2 = 2.50 **2-3 = 1.75** 1-3 = 3.28 3-2-1 = 99.4	0.002671	-294.17435	**3.18**
Bridge	1		1-2 = 2.62 **2-3 = 1.83** **1-3 = 1.83** 3-1-2 = 44.4	0.003392	-294.17246	3.13
Rh$_3$-O Top	6		1-2 = 2.52 1-3 = 2.58 2-3 = 2.51 **4-3 = 1.75** 4-3-1 = 100.0	0.003586	-403.74293	3.23
Bridge	6		1-2 = 1-3 = 2.48 2-3 = 2.70 **2-4 = 3-4 = 1.92** 2-3-4 = 45.4	0.003358	-403.75788	**3.63**
Rh$_4$-O Top	1		1-3 = 1-4 = 3-4 = =2.52 1-2 = 2.46 **2-5 = 1.72** 5-2-1 = 143.2 5-2-4 = 5-2-3 = 143.7	0.005880	-513.30528	2.95
Bridge	1		1-2 = 2-3 = 3-4 =2.50 **4-5 = 2-5 = 1.90** 2-4 = 3.01 5-4-2 = 37.7	0.006031	-513.33376	**3.73**
Rh$_5$-O Hollow	4		1-2 = 2.70 2-3 = 3.14 2-4 = 2.67 1-4 = 2.61 3-5 = 2.53 **3-6 = 1.94** **2-6 = 1.97** **4-6 = 1.99**	0.006436	-622.89470	3.69
Bridge	4		1-2 = 2.63 2-3 = 2.69 2-4 = 2.57 1-4 = 2.63 3-5 = 2.61 **1-6 = 5-6 = 1.88** 5-6-1 = 101.8	0.006042	-622.90391	**3.94**
Rh$_6$-O Bridge	1		1-3 = 1-5 = 2-3 = 2-5 = 2.48 4-6 = 2.43 **7-6 = 7-4 = 1.93** 7-4-6 = 50.8	0.007533	-732.44673	3.67

[a] Shortest Rh−O bond distances and BE for the most stable systems are indicated in bold.

Nayak et al.,[44] although the bond length difference found by these authors was only 0.02 Å. For the triangular bipyramid Rh$_5$, the bond lengths Rh1−Rh2, Rh2−Rh3, and Rh3−Rh1 are equal to 2.6 Å (Table 1), and they all decrease approximately by 0.1 Å when H adsorbs on a tilted top site (Table 2), whereas the distances between Rh5 and Rh4 and the central (Rh1, Rh2,

and Rh3) atoms are elongated by approximately 0.02 Å. In addition, the Rh−Rh bond length of the pair connected to H is significantly elongated by 0.17 Å with respect to its original length in Rh$_5$.
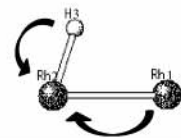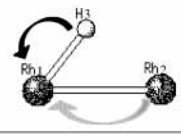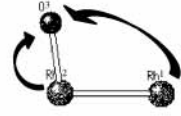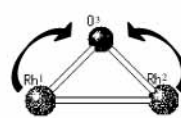
Top and bridge ground-state structures were found for Rh$_6$−H (Table 2). Adsorption on bridge, a quartet, is the most stable

TABLE 4: Charge Distribution and Electron Population for Single Atoms and the Most Stable Rh−X (X = H, O) Configurations[a]

Species		Rh	Adatom	e- Transfer
H	charge	0.000		
	s	1.00		
	p	0.00		
	d	0.00		
O	charge	0.000		
	s	4.00		
	p	4.00		
	d	0.00		
Rh	charge	0.000		
	s	3.00		
	p	6.00		
	d	8.00		
Rh - H	charge	0.03	-0.03	
	s	2.78	1.03	
	p	6.07		Rh ⤸ H
	d	8.12		
Rh - O	charge	0.38	-0.38	
	s	2.35	3.96	
	p	6.13	4.42	Rh ⤸ O
	d	8.15		

[a] A schematic electron-transfer representation is included. Gray scale has been use to denote strength of the donation (black = strongest).

TABLE 5: Charge Distribution and Electron Population for Rh$_2$ and the Most Stable Rh$_2$−X (X = H, O) Configurations[a]
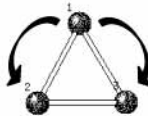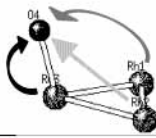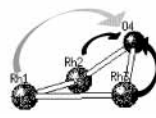
Species		Rh 1	Rh 2	Adatom	e- Transfer
Rh$_2$	charge	0.00	0.00		
	s	2.57	2.57		
	p	6.05	6.05		
	d	8.38	8.38		
Rh$_2$ – H Top	charge	0.06	-0.12	0.06	
	s	2.72	2.66	0.94	
	p	6.09	6.11		
	d	8.13	8.35		
Rh$_2$ – H Tilted top	charge	-0.09	0.03	0.06	
	s	2.59	2.74	0.94	
	p	6.10	6.11		
	d	8.41	8.11		
Rh$_2$ – O Top	charge	0.19	0.19	-0.38	
	s	2.48	2.63	3.96	
	p	6.04	6.22	4.42	
	d	8.29	7.96		
Rh$_2$ – O Bridge	charge	0.23	0.23	-0.46	
	s	2.49	2.49	3.95	
	p	6.09	6.09	4.50	
	d	8.20	8.20		

[a] A schematic electron-transfer representation is included. Gray scale has been use to denote strength of the donation (black = strongest).

with a binding energy 0.18 eV stronger than that of the on-top adsorption. In contrast to the cases of Rh$_2$, Rh$_4$, and Rh$_5$, in which the cluster symmetry is lost because of the presence of the adsorbate, the distortion induced by H adsorbed on the Rh$_6$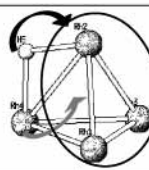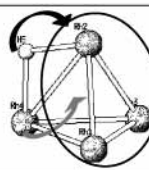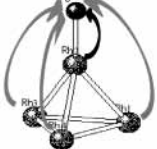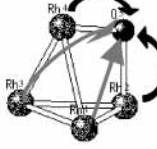 square bipyramid (Table 1) yields higher-order symmetry on the Rh$_6$−H complex. An interesting phenomenon has been recently reported in relation to Rh$_6$ clusters supported on zeolite cavities, in which via a "reverse spillover" process, H atoms

TABLE 6: Charge Distribution and Electron Population for Rh$_3$ and the Most Stable Rh$_3$−O Configurations[a]

Species		Rh 1	Rh 2	Rh 3	Adatom	e- Transfer
Rh$_3$	charge	0.04	-0.02	-0.02		
	s	2.76	2.70	2.70		
	p	6.08	6.11	6.11		
	d	8.14	8.20	8.20		
Rh$_3$ − O Top	charge	0.13	0.02	0.22	-0.37	
	s	2.55	2.66	2.64	3.97	
	p	6.08	6.10	6.27	4.40	
	d	8.24	8.22	7.88		
Rh$_3$ − O Bridge	charge	0.04	0.22	0.22	-0.48	
	s	2.68	2.51	2.51	3.94	
	p	6.10	6.18	6.18	4.54	
	d	8.18	8.09	8.09		

[a] A schematic electron-transfer representation is included. Gray scale has been use to denote strength of the donation (black = strongest).

TABLE 7: Charge Distribution and Electron Population for Rh$_4$ and the Most Stable Rh$_4$−X (X = H, O) Configurations[a]

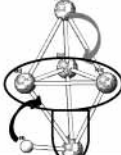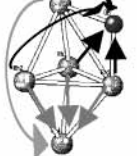| Species		Rh 1	Rh 2	Rh 3	Rh 4	Adatom	e- Transfer
Rh$_4$	charge	0.00	0.00	0.00	0.00		
	s	2.62	2.62	2.62	2.62		
	p	6.12	6.12	6.12	6.12		
	d	8.26	8.26	8.26	8.26		
Rh$_4$ − H Bridge	charge	-0.01	-0.02	-0.01	0.01	0.03	
	s	2.61	2.54	2.61	2.48	0.97	
	p	6.13	6.17	6.13	6.16		
	d	8.27	8.31	8.27	8.34		
Rh$_4$ − O Top	charge	0.07	0.21	0.07	0.07	-0.41	
	s	2.57	2.67	2.57	2.57	3.97	
	p	6.09	6.33	6.09	6.09	4.44	
	d	8.27	7.79	8.27	8.27		
Rh$_4$ − O Bridge	charge	0.01	0.24	0.01	0.24	-0.52	
	s	2.64	2.46	2.64	2.46	3.93	
	p	6.11	6.21	6.11	6.21	4.59	
	d	8.23	8.09	8.23	8.09		

[a] A schematic electron-transfer representation is included. Gray scale has been use to denote strength of the donation (black = strongest).

leave the support and become attached to Rh$_6$ clusters in bridge positions.[46] Vayssilov et al.[46] report Rh$_6$(3H)/zeolite structures where each of three H atoms bridge to a Rh−Rh bond of Rh$_6$ with Rh−Rh distances in the range 2.60−2.67 Å, which are very comparable with our results for the last structure Rh$_6$H shown in Table 2, in which all of the Rh−Rh bond lengths are approximately 2.60 Å, except for the Rh−Rh pair bonded to H (2.76 Å). Although it is possible that when three atoms are bonded, such Rh−Rh bond elongation becomes reduced, an important difference between our calculation and that from Vassilov et al. is that they have included the zeolite support, which determines a change in the oxidation state in the metal cluster. Their reported[46] calculated Rh−H bond distance is 1.76 Å, which also compares well with our values of 1.74 and 1.80 Å (Table 2). The same authors also report Rh−O interactions, which are discussed in relation to Table 3.

In summary, our study did not yield any stable structure in which H adsorbs to a Rh$_n$ cluster occupying hollow sites. Thus, in these small clusters, H can adsorb both on top and bridge with bridgelike sites being slightly more stable, in agreement with theoretical and experimental studies at least for the largest cluster.[46] The binding energies of H attached to Rh$_n$ clusters on top sites increase with the number of atoms, except for Rh$_5$H, which exhibits a lower energy than RhH and Rh$_2$H, which can be attributed to the fact that although all of the reported complexes are local minima, we cannot guarantee that they are the true global minima and therefore alternative geometries could exist that provide stronger adsorption energy in the case of Rh$_5$H.
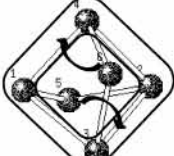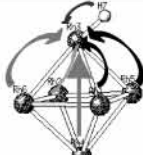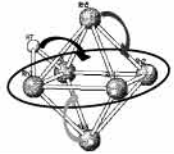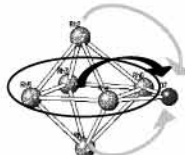
Table 3 illustrates that oxygen chemisorbs to the Rh atom with a binding energy of −3.80 eV, 1.15 eV stronger than that of Rh−H (Table 2). The ground state corresponding to Rh−O

TABLE 8: Charge Distribution and Electron Population for Rh$_5$ and the Most Stable Rh$_5$–X (X = H, O) Configurations[a]

Species		Rh 1	Rh 2	Rh 3	Rh 4	Rh 5	Adatom	e- Transfer
Rh$_5$	*charge*	0.01	0.01	0.01	-0.01	-0.02		
	s	2.58	2.58	2.58	2.51	2.62		
	p	6.17	6.17	6.17	6.13	6.15		
	d	8.25	8.25	8.25	8.37	8.24		
Rh$_5$–H	*charge*	-0.01	-0.01	-0.01	-0.05	0.02	0.06	
Tilted	*s*	2.53	2.60	2.60	2.49	2.47	0.95	
top	*p*	6.26	6.21	6.21	6.08	6.14		
	d	8.22	8.20	8.20	8.41	8.44		
Rh$_5$–O	*charge*	0.07	0.18	0.19	0.07	-0.01	-0.50	
Hollow	*s*	2.57	2.44	2.45	2.49	2.56	3.93	
	p	6.19	6.23	6.19	6.18	6.10	4.57	
	d	8.18	8.16	8.17	8.27	8.34		
Rh$_5$–O	*charge*	0.17	0.10	0.08	-0.02	0.16	-0.49	
Bridge	*s*	2.54	2.54	2.55	2.62	2.46	3.94	
	p	6.24	6.16	6.17	6.12	6.20	4.55	
	d	8.05	8.20	8.20	8.28	8.18		

[a] A schematic electron-transfer representation is included. Gray scale has been use to denote strength of the donation (black = strongest).

TABLE 9: Charge Distribution and Electron Population for Rh$_6$ and the Most Stable Rh$_6$–X (X = H, O) Configurations[a]

Species		Rh1	Rh 2	Rh 3	Rh 4	Rh 5	Rh 6	Adatom	e- Transfer
Rh$_6$	*charge*	-0.01	-0.01	-0.01	-0.01	0.02	0.02		
	s	2.52	2.52	2.53	2.53	2.57	2.57		
	p	6.28	6.28	6.26	6.26	6.20	6.17		
	d	8.17	8.17	8.32	8.32	8.11	8.22		
Rh$_6$–H	*charge*	0.08	0.01	-0.24	0.02	0.06	0.03	0.05	
Top	*s*	2.50	2.53	2.59	2.53	2.53	2.51	0.96	
	p	6.18	6.20	6.39	6.18	6.21	6.24		
	d	8.24	8.26	8.25	8.28	8.20	8.22		
Rh$_6$–H	*charge*	-0.01	-0.01	-0.06	-0.02	0.04	0.00	0.06	
Bridge	*s*	2.46	2.54	2.48	2.55	2.44	2.53	0.94	
	p	6.23	6.24	6.28	6.18	6.28	6.19		
	d	8.32	8.23	8.30	8.29	8.24	8.28		
Rh$_6$–O	*charge*	0.04	0.04	0.07	0.13	0.07	0.13	-0.48	
Bridge	*s*	2.51	2.51	2.50	2.42	2.50	2.42	3.94	
	p	6.20	6.20	6.16	6.35	6.16	6.35	4.54	
	d	8.24	8.24	8.27	8.09	8.27	8.09		

[a] A schematic electron-transfer representation is included. Gray scale has been use to denote strength of the donation (black = strongest).

is a spin quartet with a bond length of 1.76 Å and a calculated Rh–O stretching frequency of 787 cm^{-1} (scaling factor of 0.9573[42] has been applied). The calculated binding energy is −3.49 eV, which is below the experimental value of −4.2 eV reported from mass spectrometry measurements.[47] However, as discussed for Rh$_2$, it is not clear whether the dissociation

obtained in the experiment ends with atomic Rh in its ground or in its first excited state, which would change the reference and modify the value of the binding energy.

On-top and bridge optimized geometries were found for each of the Rh$_2$–O, Rh$_3$–O, and Rh$_4$–O systems. Rh$_2$–O on-top adsorbs with a binding energy 0.05 eV stronger than that of
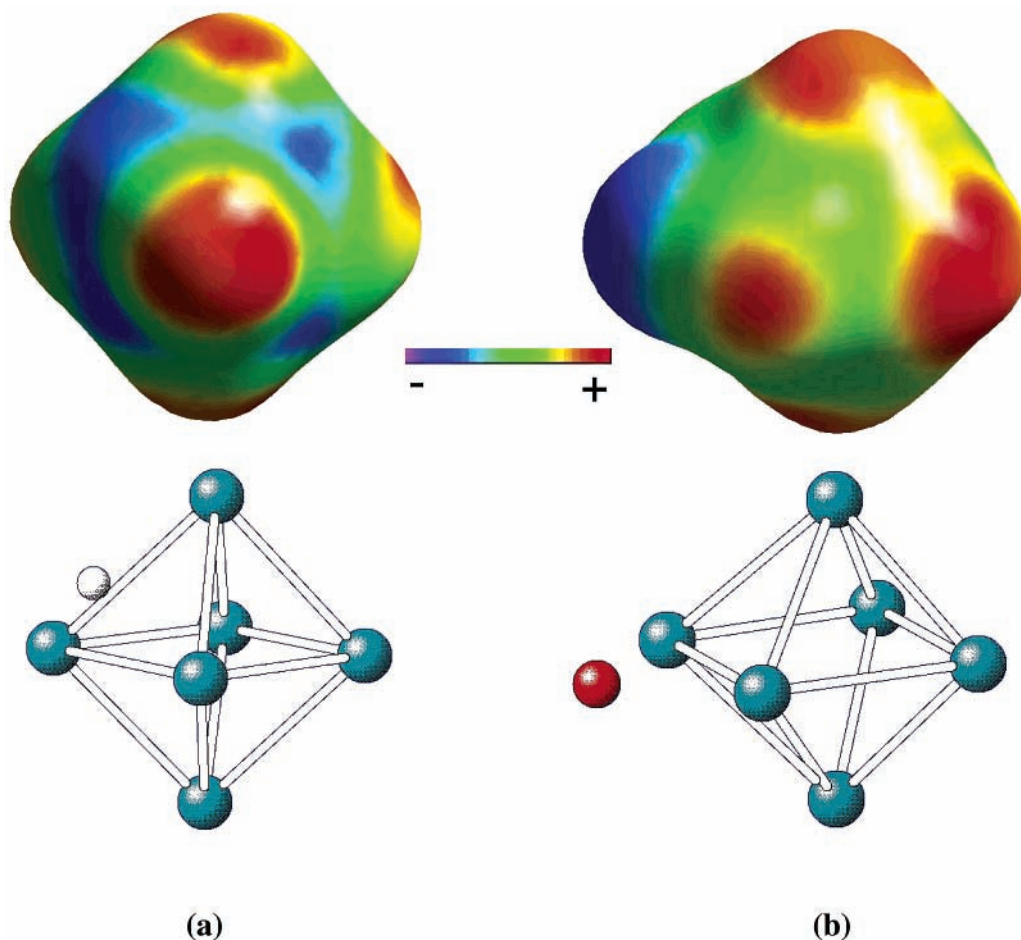
Figure 1. Electrostatic potential energy surfaces mapped over an isodensity of 0.017 eV corresponding to (a) Rh_6–H and (b) Rh_6–O, both corresponding to adsorptions on bridge sites.

Rh_2–O bridge adsorption. As found with adsorbed H, the Rh–Rh bond length increases from 2.30 to 2.50 Å for the on-top adsorption and to 2.62 Å for the bridge case, with respect to that in Rh_2 (Table 1).

On the other hand, Rh_3–O on-top is 0.40 eV less stable than the bridge configuration, and both spin multiplicities are sextets. All of the Rh–Rh distances of Rh_3–O increase with respect to those in the Rh_3 cluster. In the on-top structure, the O atom became adsorbed to one of the Rh atoms in the base of the isosceles triangle, causing a rearrangement of the Rh_3 cluster to an equivalent C_{2v} geometry. In the bridge geometry, O adsorbs also to the base of the isosceles triangle, inducing an elongation of the Rh–Rh bond length to 2.70 Å, whereas the other two Rh–Rh bond lengths are shortened.

The energetic pattern found in Rh_4–O is similar to that in Rh_3–O; the on-top adsorption is 0.78 eV less stable than the bridge case, both having singlet spin multiplicities. When O adsorbs on a bridge site of Rh_4, a significant elongation is observed in the Rh–Rh bond connected to the O atom (from 2.48 to 3.01 Å), similarly to H-adsorption on bridge of Rh_4 and also to O-adsorption on bridge of Rh_3. The other Rh–Rh bond lengths are also slightly increased by 0.02 Å.

Rh_5–O (on hollow adsorption) is 0.25 eV less stable than O adsorbed in a bridge site, and both are quartets. Upon adsorption on a hollow site, the bond lengths Rh1–Rh2, Rh2–Rh3, and Rh3–Rh1, as well as the distances between Rh5 and Rh4 and the central (Rh1, Rh2, and Rh3) atoms in Rh_5–O, are more elongated than in the case of bridge adsorption (Table 3), for which all of the Rh–Rh bond lengths not in contact with the

adsorbate are equally stretched by more than 0.1 Å. In addition, the distances between Rh5 and Rh4 and the central (Rh1, Rh2, and Rh3) atoms in Rh_5–O (bridge) are also elongated; this is the same effect found for bridge H-adsorption on Rh_5.

The last case investigated, Rh_6–O adsorption on bridge, has a binding energy of −3.67 eV with singlet spin multiplicity, showing also a strong effect on the metal cluster geometry, which is relevant to certain technological applications. As mentioned above, zeolites have been proposed as templates where transition metal clusters are inserted for catalysis applications.[46,48] Zeolite atoms (H, O, and others) located in positions where they can strongly interact with the metal cluster may contribute to alter their geometry and consequently their catalytic properties.[48] Experimental measurements[49] indicate that the distance RhO in such clusters is on the order of 2.10–2.17 Å, which compares well with our calculated value of 1.93 Å for O adsorbed on bridge site of Rh_6. Changes in geometry such as those illustrated for Rh_6–H and Rh_6–O, where the presence of H and O remove the distortion found in the square bipyramid optimized structure of the pure Rh_6 cluster, may be crucial for tailoring metal clusters to specific geometries for catalysis applications.

On the basis of the results of this section, it can be concluded that bridge sites are the preferred sites in most cases for O adsorption in small rhodium clusters. The case of H is less conclusive; the small size of the adsorbate may favor top or bridge sites depending on the metal cluster morphology. As discussed for Rh_nH, the adsorption energies for O adsorbed on bridge sites in Rh_n clusters increase steadily as a function of

the number of atoms in the metal clusters, except for Rh$_6$O with a binding energy 0.27 eV lower than that of Rh$_5$O. Besides, an oscillation in the value of the binding energy of O to Rh$_n$ as a function of the number of atoms in the cluster is observed for the case of on-top adsorption. Although oscillations in some clusters properties are observed as a function of the number of atoms,[45,50,51] we suggest that these apparent anomalies could be because some of the structures may not be the absolute global minima.

To further understand the interactions of metal cluster–adsorbate, it is useful to analyze charge transfer given by Mulliken population.[52–54] Table 4 illustrates that charge transfer in Rh–X occurs from the metal to the adatom X (X = H, O). In Rh–H, charge is transferred from the s orbital of Rh to the d and p orbitals of Rh and to the s orbital of H. A similar process takes place from the d orbital of Rh to the d and p Rh orbitals and to the p orbital of O in the Rh–O cluster, where a significant charge transfer is observed from Rh to the O atom.

In Rh$_2$–H clusters, irrespective of the H adsorption site, charge transfer occurs (Table 5) from both Rh and H to the Rh atom closer to H. The Rh–Rh charge transfer is less pronounced (gray arrow, Table 5) but still noticeable when adsorption takes place in the tilted top site. However, the amount of charge transfer coming from H is the same in both cases. The charge flow in Rh$_2$–H (Table 5) originates at the s orbital of H and d orbital from Rh toward the second Rh atom. In Rh$_2$–O clusters, irrespective of the adsorption site, charge transfer occurs equally from both Rh atoms to O. For on-top Rh$_2$–O, the s and p populations of Rh2 (the Rh atom bonded to O) increase, whereas the d population decreases. In the case of Rh$_2$–O (bridge), the p population of Rh atoms slightly increases while the others decrease. Higher charge transfer is observed when the O adsorption site is bridge (which also have higher binding energies) than when the adsorption site is on top sites.

The charge transfer in Rh$_3$–O (Table 6) is also from the Rh atoms to the O. The two Rh atoms involved in the binding to O in a top tilted site contribute with electron donation to the oxygen p orbital. In the case of O adsorption on a bridge site, the Rh atom far from O almost does not contribute at all, although a small redistribution is observed in its electronic population. The p populations of Rh2 and Rh3 (the Rh atoms bonded to O) increase in a small amount, while their other populations decrease, thus indicating charge transfer from d orbitals of the metal atoms to the p orbitals of O.

For Rh$_4$–H (Table 7), charge is transferred from Rh4 (one of the Rh atoms bonded to H) and H to the other Rh atoms in the cluster, whereas Rh2 (the other Rh atom bonded to H) bears the highest negative charge in the mixed cluster. The s populations of the two metal atoms connected to H decrease, while their p and d populations increase. On the other hand, charge transfer occurs from the Rh atoms to O irrespective of the O adsorption site in Rh$_4$–O.

Table 8 shows similar trends as those described in Tables 4–7 for Rh$_5$–X clusters. Overall, the interaction with H in Rh$_5$–H can be described as a charge donation from H and the Rh atom located farther from H than the other Rh atoms. The Rh$_5$–O clusters follow the same electronic and charge-transfer characteristics described for Rh$_n$–O ($n = 1-4$).

Rh$_6$–H and Rh$_6$–O (Table 9) are probably the clearest illustrations of the adsorption pattern observed in these and the smaller clusters. In Rh$_6$–H top, the Rh atom bonded to H (Rh3) receives the charge flow from all its neighbor Rh atoms favoring the binding with the adsorbate. In Rh$_6$–O, the two Rh atoms involved in the bridge binding to O donate electrons to the

adsorbate p orbitals. To illustrate the characteristics of the metal–adatom interactions in these small clusters, Figure 1 displays the electrostatic potential surface corresponding to Rh$_6$–H (a) and Rh$_6$–O (b), both corresponding to adsorptions on bridge sites. When H adsorbs on a bridge site of Rh$_6$, electron delocalization is observed, whereas when oxygen adsorbs on a bridge site of Rh$_6$ (Figure 1b), the electrons are localized in the oxygen vicinity.

4. Conclusions

DFT calculations indicate that bridge sites are preferred in most cases for O adsorption in small Rh$_n$ clusters. The case of H is not that conclusive; the small size of the adsorbate may favor top or bridge sites depending on the metal cluster morphology, bridge sites being slightly more stable. However, the bridge adsorption of H in hexarhodium clusters is in agreement with structures inferred from experiments and calculated for Rh$_6$ clusters supported in zeolite cavities.

In Rh$_n$–H, when $n = 1$, the charge transfer occurs from the metal to the adatom, whereas for $n = 2-6$, irrespective of the H adsorption site, charge transfer occurs from one Rh and H to the rest of the Rh atoms in the cluster. In the case of Rh$_n$–O ($n = 1-6$) clusters, charge transfer occurs from Rh atoms to O irrespective of the O adsorption site and mostly involves d orbitals from the metal clusters and p orbitals of O.

Significant changes in the clusters geometry upon adsorption of H and O, such as those illustrated for Rh$_6$–H and Rh$_6$–O, where the presence of the adsorbates removes the distortion found in the square bipyramid optimized structure of the pure Rh$_6$ cluster, may be crucial for tailoring metal clusters to specific geometries for catalysis applications.

References and Notes

(1) Reddy, B. V.; Nayak, S. K.; Khanna, S. N.; Rao, B. K.; Jena, P. Physics of Nickel Clusters. 2. Electronic Structure and Magnetic Properties. *J. Phys. Chem. A* **1998**, *102*, 1748.

(2) Reddy, B. V.; Nayak, S. K.; Khanna, S. N.; Rao, B. K.; Jena, P. Electronic Structure and Magnetism of Rh$_n$ ($n = 2-13$) Clusters. *Phys. Rev. B* **1999**, *59*, 5214.

(3) Cox, A. J.; Louderback, J. G.; Aspeal, S. E.; Bloomfield, L. A. Magnetism in 4d-Transition Metal-Clusters. *Phys. Rev. B* **1994**, *49*, 12295.

(4) Jensen, F. *Introduction to Computational Chemistry*; Wiley: Chichester, U.K., 1999.

(5) Nakatsuji, N.; Nakai, H.; Hada, M. Catalytic Reactions of Transition Metal Clusters and Surfaces from Ab Initio Theory. In *Metal–Ligand Interactions: from Atoms, to Clusters, to Surfaces*; Salahub, D. R., Russo, N., Eds.; Kluwer Academic: Dordrecht, The Netherlands, 1992; p 251.

(6) Knickelbein, M. B. Reactions of transition metal clusters with small molecules. *Annu. Rev. Phys. Chem.* **1999**, *115*, 50.

(7) Somorjai, G. A. *Introduction to Surface Chemistry and Catalysis*; John Wiley & Sons, Inc.: New York, 1994.

(8) Tamura, H.; Sasahara, A.; Tanaka, K. I. Cyclic Voltammogram of Rh(100), Pt-Deposited Rh(100) and Chemically Reconstructed Pt/Rh(100) Surfaces. *J. Electroanal. Chem.* **1995**, *381*, 95.

(9) Chien, C. H.; Blaisten-Barojas, E. Many-Body Potential and Structure for Rhodium Clusters. *J. Chem. Phys.* **2000**, *112*, 2301.

(10) Chien, C. H.; Blaisten-Barojas, E.; Pederson, M. R. Magnetic and Electronic Properties of Rhodium Clusters. *Phys. Rev. A* **1998**, *58*, 2196.

(11) Jinlong, Y.; Toigo, F.; Kelin, W. The Structural, Electronic, and Magnetic Properties of Small Rhodium Clusters. *Phys. Rev. B* **1994**, *50*, 7915.

(12) Sun, H.; Ren, Y.; Luo, Y. H.; Wang, G. Geometry, Electronic Structure, and Magnetism of Rh$_n$ (n = 9, 13, 15, 17, 19) clusters. *Physica B* **2001**, *293*, 260.

(13) Lacaze-Dufour, C.; Mineva, T.; Russo, N. Density Functional Study of the Structural, Electronic, and Magnetic Properties of Neutral and Charged Rhodium Clusters up to Tetramer. *Int. J. Quantum Chem.* **2001**, *85*, 162.

(14) Kohl, A.; Labich, S.; Taglauer, E.; Knozinger, H. Agglomeration of supported rhodium on model catalysts. *Surf. Sci.* **2000**, *454*, 974.

(15) Wilke, S.; Henning, D.; Lober, R. Ab Initio Calculations of Hydrogen Adsorption on (100) Surfaces of Palladium and Rhodium. *Phys. Rev. B* **1994**, *50*, 2548.

(16) Feibelman, P. J. First-Principles Calculations of Adatom Binding and Interaction on Rh(001). *Phys. Rev. B* **1991**, *43*, 9452.

(17) Mavrikakis, M.; Rempel, J.; Greeley, J.; Hansen, L. B.; Norskov, J. K. Atomic and Molecular Adsorption on Rh(111). *J. Chem. Phys.* **2002**, *117*, 6737.

(18) Richter, L. J.; Ho, W. Vibrational modes of hydrogen adsorbed on Rh(100) and their relevance to desorption kinetics. *J. Vac. Sci. Technol., A* **1987**, *A5*, 453.

(19) Baraldi, A.; Cerdá, J.; Martín-Gago, J. A.; Comelli, G.; Lizzit, S.; Paolucci, G.; Rosei, R. Oxygen Induced Reconstruction of the Rh(100) Surface: General Tendency Towards Threefold Oxygen Adsorption Site on Rh Surfaces. *Phys. Rev. Lett.* **1999**, *82*, 4874.

(20) Alfe, D.; De Gironcoli, S.; Baroni, S. The Reconstruction of Nickel and Rhodium (001) Surfaces Upon Carbon, Nitrogen, or Oxygen Adsorptions. *Surf. Sci.* **1999**, *437*, 18.

(21) Shen, Y. G.; Qayyum, A.; O'Connor, D. J.; King, B. V. Oxygen-Induced Surface (2 × 2)p4g Reconstruction of Rh(001). *Phys. Rev. B* **1998**, *58*, 10025.

(22) Hansen, E. W.; Neurock, M. First-principles-based Monte Carlo methodology applied to O/Rh(100). *Surf. Sci* **2000**, *464*, 91.

(23) Ganduglia-Pirovano, M. V.; Scheffler, M. Structural and Electronic Properties of Chemisorbed Oxygen on Rh(111). *Phys. Rev. B* **1999**, *59*, 15533.

(24) *Recent Developments and Applications of Modern Density Functional Theory*; Seminario, J. M., Ed.; Elsevier Science Publishers: Amsterdam, 1996; Vol. 4.

(25) Parr, R. G.; Yang, W. *Density Functional Theory of Atoms and Molecules*; Oxford University Press: Oxford, U.K., 1989.

(26) Hay, P. J.; Wadt, W. R. Ab initio effective core potentials for molecular calculations. Potentials for the transition metal atoms Sc to Hg. *J. Chem. Phys.* **1985**, *82*, 270.

(27) Wadt, W. R.; Hay, P. J. Ab initio effective core potentials for molecular calculations. Potentials for main group elements Na to Bi. *J. Chem. Phys.* **1985**, *82*, 284.

(28) Becke, A. D. A new mixing of Hartree−Fock and local density-functional theories. *J. Chem. Phys.* **1993**, *98*, 1372.

(29) Becke, A. D. Density functional thermochemistry II. The effect of the Perdew-Wang generalized gradient correlation correction. *J. Chem. Phys.* **1992**, *97*, 9173.

(30) Becke, A. D. Density-functional thermochemistry. III. The role of exact exchange. *J. Chem. Phys.* **1993**, *98*, 5648.

(31) Perdew, J. P. Unified theory of exchange and correlation beyond the local density approximation. In *Electronic Structure of Solids*; Eschrig, H., Ed.; Akademie Verlag: Berlin, 1991.

(32) Neyman, K. M.; Pacchioni, G.; Rosch, N. Adsorption complexes on oxides: density functional model cluster studies. In *Recent developments and applications of modern density functional theory*; Seminario, J. M., Ed.; Elsevier: Amsterdam, 1996; p 569.

(33) Hehre, W. J.; Radom, L.; Schleyer, P. v. R.; Pople, J. A. *Ab Initio Molecular Orbital Theory*; John Wiley & Sons: New York, 1986.

(34) Frisch, M. J.; Trucks, G. W.; Schlegel, H. B.; Scuseria, G. E.; Robb, M. A.; Cheeseman, J. R.; Zakrzewski, V. G.; Montgomery, J. A., Jr.; Stratmann, R. E.; Burant, J. C.; Dapprich, S.; Millam, J. M.; Daniels, A. D.; Kudin, K. N.; Strain, M. C.; Farkas, O.; Tomasi, J.; Barone, V.; Cossi, M.; Cammi, R.; Mennucci, B.; Pomelli, C.; Adamo, C.; Clifford, S.; Ochterski, J.; Petersson, G. A.; Ayala, P. Y.; Cui, Q.; Morokuma, K.; Malick, D. K.; Rabuck, A. D.; Raghavachari, K.; Foresman, J. B.; Cioslowski, J.; Ortiz, J. V.; Stefanov, B. B.; Liu, G.; Liashenko, A.; Piskorz, P.; Komaromi, I.; Gomperts, R.; Martin, R. L.; Fox, D. J.; Keith, T.; Al-Laham, M. A.; Peng, C. Y.; Nanayakkara, A.; Gonzalez, C.; Challacombe, M.; Gill, P. M. W.; Johnson, B. G.; Chen, W.; Wong, M. W.; Andres, J. L.; Head-Gordon, M.; Replogle, E. S.; Pople, J. A. *Gaussian 98*, revision A.11; Gaussian, Inc.: Pittsburgh, PA, 1998.

(35) Peng, C.; Ayala, P. Y.; Schlegel, H. B.; Frisch, M. J. Using redundant internal coordinates to optimize equilibrium geometries and transition states. *J. Comput. Chem.* **1996**, *17*, 49.

(36) Moore, C. E. *Atomic Energy Levels*; Circular 467; National Bureau of Standards: Gaithersburg, MD, 1958; Vol. III.

(37) Yang, L.; DePristo, A. E. On the compact structure of small fcc metal clusters. *J. Catal.* **1994**, *149*, 223.

(38) Langenberg, J. D.; Morse, M. D. The bond energy of Rh$_2$. *J. Chem. Phys.* **1998**, *108*, 2331.

(39) Wang, H.; Haouari, H.; Craig, R.; Liu, Y.; Lombardi, J. R.; Lindsay, D. M. Spectroscopy of Mass-Selected Rhodium Dimers in Argon Matrices. *J. Chem. Phys.* **1997**, *106*, 2101.

(40) Gingerich, K. A.; Cocke, D. L., *Chem. Commun.* **1972**, *1*, 536.

(41) Cocke, D. L.; Gingerich, K. A., *J. Chem. Phys.* **1974**, *60*, 1958.

(42) Halls, M. D.; Velkovski, J.; Schlegel, H. B. Harmonic Frequency scaling factors for Hartree−Fock, S-VWN, B-LYP, B3-LYP, B3-PW91 and MP2 with the Sadlej pVTZ electric property basis set. *Theor. Chem. Acc.* **2001**, *105*, 413.

(43) Das, K. K.; Balasubramanian, K. Potential energy surfaces of eight low-lying electronic states of Rh$_3$. *J. Chem. Phys.* **1990**, *93*, 625.

(44) Nayak, S. K.; Weber, S. E.; Jena, P.; Wildberger, K.; Zeller, R.; Dederichs, P. H.; Stepanyuk, V. S.; Hergert, W. Relationship between magnetism, topology, and reactivity of Rh clusters. *Phys. Rev. B* **1997**, *56*, 8849.

(45) Li, T.; Balbuena, P. B. Computational studies of the interactions of oxygen with platinum clusters. *J. Phys. Chem. B* **2001**, *105*, 9943.

(46) Vayssilov, G. N.; Gates, B. C.; Rotsch, N. Oxidation of supported rhodium clusters by support hydroxy groups. *Angew. Chem., Int. Ed.* **2003**, *42*, 1391.

(47) Huber, K. P.; Herzberg, G. *Molecular spectra and molecular structure. IV. Constants of diatomic molecules*; Van Nostrand Reinhold Company: New York, 1978.

(48) Reifsnyder, S. N.; Otten, M. M.; Lamb, H. H. Nucleation and Growth of Pd Clusters in Mordenite. *Catal. Today* **1998**, *39*, 317.

(49) Weber, W. A.; Gates, B. C. Hexarhodium clusters in NaY zeolite: Characterization by infrared and extended X-ray absorption fine structure spectrocopies. *J. Phys. Chem. B* **1997**, *101*, 10423.

(50) Balbuena, P. B.; Derosa, P. A.; Seminario, J. M. Density functional theory study of copper clusters. *J. Phys. Chem. B* **1999**, *103*, 2830.

(51) Derosa, P. A.; Seminario, J. M.; Balbuena, P. B. Properties of Small Bimetallic Ni−Cu Clusters. *J. Phys. Chem. A* **2001**, *105*, 7917.

(52) Mulliken, R. S. Electronic poputaion analysis on LCAO-MO molecular wave functions. I, *J. Chem. Phys.* **1955**, *23*, 1833.

(53) Mulliken, R. S. Electronic population analysis on LCAO-MO molecular wave functions. II. Overlap populations, bond orders, and covalent bond energies. *J. Chem. Phys.* **1955**, *23*, 1841.

(54) Mulliken, R. S. Electronic population analysis on LCAO-MO molecular wave functions. III Effects of hybridization on overlap and gross AO populations. *J. Chem. Phys.* **1955**, *23*, 2338.